Available online at www.sciencedirect.com
ScienceDirect
Journal of Sound and Vibration 321 (2009) 45–64
JOURNAL OF SOUND AND VIBRATION
www.elsevier.com/locate/jsvi

# Effects of partial constrained viscoelastic layer damping parameters on the initial transient response of impacted cantilever beams: Experimental and numerical results

Daniel Granger, Annie Ross*

*CREPEC, Department of Mechanical Engineering, École Polytechnique de Montréal, CP 6079 succ. Centre-ville, Montréal (Qué), Canada H3C 3A7*

Received 21 December 2007; received in revised form 12 June 2008; accepted 18 September 2008
Handling Editor: S. Bolton
Available online 12 November 2008

**Abstract**

The effects of partial constrained viscoelastic layer damping on the first milliseconds of the transient vibration of an impacted beam is studied using an analytical model. The viscoelastic properties of the core are frequency dependent and the shear modulus is modelled using a Prony Series. The equations of motion of the system are obtained using Lagrange's equations. The equations of motion are converted in the frequency domain using a Fourier Transform and they are solved for frequency displacements using the assumed modes method. They are then converted back in the time domain using an inverse Fourier Transform. The technique is validated for transient responses using experimental impact force signals. The numerical results are in good agreement with experimental data. Four partial constrained viscoelastic layer damping parameters are studied: the length, the placement, the viscoelastic layer thickness and the constraining layer thickness. It turns out that the length of the partial constrained viscoelastic layer damping has the most important effect on the initial transient displacement while the viscoelastic layer thickness has little effect. Noncausal effects in the model are discussed and are mainly induced when the partial constrained viscoelastic layer damping treatment is poorly effective.


## 1. Introduction

Unwanted vibrations are a source of many problems. For instance, the riveting process used in aircraft assembly necessarily induces strong impacts on structures. These impacts are likely to produce transient vibrations which are responsible for making powerful noise. This is specially true for large and flexible structures that can experience severe acoustical radiation. This may cause work-related injuries, even when workers benefit from auditory protection equipment. Hence, it is important to develop a damping treatment which would effectively reduce transient vibrations due to impact processes.

An ingenious way to do so is to apply on the surface of the structure a viscoelastic layer covered by another elastic layer. The elastic layer is called the constraining layer and causes the viscoelastic material to experience

*Corresponding author. Tel.: +1 514 340 4711x4591; fax: +1 514 340 4176.
*E-mail address:* annie.ross@polymtl.ca (A. Ross).

0022-460X/$ - see front matter © 2008 Elsevier Ltd. All rights reserved.
doi:10.1016/j.jsv.2008.09.039

shear deformation which increases the energy dissipation in the viscoelastic layer. This kind of passive treatment is called constrained layer damping. However, in order to limit added mass and for cost considerations, damping treatments covering an entire structure have been replaced by partial constrained viscoelastic layer damping. Moreover, it was shown that constrained layer damping is not necessarily more efficient than partial constrained viscoelastic layer damping [1]. From a practical point of view, partial constrained viscoelastic layer damping can either be applied to existing structures or be part of the design process.

This paper deals with the effects of partial constrained viscoelastic layer damping on the transient response of impacted beams. There are good reasons to study beams. For instance, the behavior of beams is mathematically well known. They have been studied for a long time and they are the first step to understand the behavior of more complex structures. Also, it is easy to verify theoretical results by means of experiments.

The harmonic behavior of constrained layer damping and partial constrained viscoelastic layer damping has been studied using analytical models by many authors. Mead and Markus proposed a model for a sandwich beam where the core layer was made of viscoelastic material [2]. They stated assumptions which have been used in many subsequent works (e.g. Refs. [3–5]). Kung and Singh are among the few authors who presented experimental data [4,5]. Huang et al. proposed the use of Lagrange's equations to derive the equation of motion of a base beam damped by a viscoelastic partial treatment [6]. They applied the assumed modes method to discretize and solve the equations. Cai et al. also used Lagrange's equations, but instead of deriving the longitudinal motion of the constraining layer using force and moment balances, they proposed to use a third set of admissible functions [7].

Design considerations of partial constrained viscoelastic layer damping treatments exist for steady-state harmonic motion only. Optimal patch design parameters were studied for the first mode of cantilever beams [8] or the first two modes [1]. Kung and Singh proposed an analytical design procedure for partial constrained viscoelastic layer damping treatment applied to a single mode at a time [5]. In all cases, the criterion used for optimal damping was a maximum modal loss factor.

Few transient analyses of viscoelastically damped structures have been conducted so far. Nashif et al. proposed a method to study single degree of freedom systems submitted to a Dirac impulse [9]. The equation of motion were converted to the frequency domain using a Fourier transform and were solved for frequency displacements. Then, the displacement was converted back into the time domain using an inverse Fourier transform.

However, time analyses have been conducted more often using finite element methods rather than analytical models. Constrained layer damping [10,11] and partial constrained viscoelastic layer damping [12] treated cantilever beams were studied, but only the damping of the first mode was analyzed using the logarithmic decrement once the forced transient response was passed and all higher modes were damped. Some of the results were compared to experiments [12].

In view of these works, some conclusions may be drawn. Many authors studied beams damped with partial constrained viscoelastic layer damping treatments using analytical models. In particular, the work done by Cai et al. effectively combines the energy approach and a discretization technique to get the equations of motion of the system, leading to a common form which is easily solvable [7]. However, much of the work was done for harmonic or steady-state response. Finite element models were proposed in the literature to understand the time response over a long period, whereas impact noises are partly due to the initial transient motion. Though some experiments were proposed to validate the natural frequencies of systems with partial constrained viscoelastic layer damping and their steady-state time response, there is a clear lack of experimental data concerning the initial forced transient response.

Finally, the viscoelastic shear properties are frequency dependent [13]. Even if frequency independent properties have been used in the past (e.g. Refs. [7,14]), this assumption received many critics because it leads to unrealistic material properties that produce inaccurate frequency peaks and noncausal response [9,15]. Moreover, the complex modulus approach is based on the assumption of cyclic motion [16–18], hence it is only valid for transient response calculations if the material shear modulus has a real time domain behavior [13]. To do so, two models are widely used: the GHM model [19,20] and the Prony Series [21,22]. Both representations ensure frequency dependence of materials and accurate behavior representation in the time domain.

For the research described in this paper there were four goals. (1) To obtain the equations of motion of a beam with a partial constrained viscoelastic layer damping using the method proposed by Cai et al. [7]. However, a Prony Series is used to make sure the viscoelastic behavior will be well suited both in the frequency and time domains. (2) To generalize the method proposed by Nashif et al. [9] for solving the equations of motion and to obtain the time response of the system submitted to a real impact. (3) To validate the time responses through experimental results. (4) To study the effects of partial constrained viscoelastic layer damping on the first few milliseconds of the transient displacement, which is responsible for initial transient impact noise.

## 2. Model

### 2.1. Geometry and displacements

The system is an impacted beam which is damped by a partial viscoelastic constrained layer (Fig. 1). The base beam has a length $L$ and arbitrary boundary conditions. In the present model, the base beam is cantilevered. The damping treatment is composed of two layers and is installed from $x_1$ to $x_2$, where $x$ is the axial coordinate of the beam. Each layer has a thickness $h_\beta$ and a density $\rho_\beta$ where $\beta = b, v$ or $c$, respectively, for the base beam, the viscoelastic layer and the constraining layer. The system has a uniform width $B$. The force is applied at $x_f$, and $x_0$ indicates the location where the response of the system is measured (not shown in Fig. 1). Prior to developing the model, some assumptions were made. They were taken directly from Mead and Markus [2] and are commonly accepted in the open literature.

(1) All displacements are small and occur in the $xz$-plane.
(2) The base beam and the constraining layer are considered purely elastic. Moreover, these two layers are only allowed to experience flexural and axial deformations. No shear deformation is taken into account; neither is the rotational inertia.
(3) The central layer is viscoelastic and can deform linearly with respect to the $z$-axis. It can experience axial and transverse displacements. Shear deformation occurs in the $xz$-plane only. Axial, compressive and tensile constraints in this layer are neglected due to the fact that Young's modulus of the viscoelastic is very small as compared to Young's moduli of the base beam and the constraining layer.
(4) As stated in Assumption (3), the viscoelastic has a constant thickness so that for a given position $x$, the transverse displacement in the $z$ direction is the same for the three layers.
(5) At the interfaces, the bonding layers are assumed to have no thickness. Perfect contact without slip is also assumed.
(6) In the frequency domain, the viscoelastic shear modulus is described using a complex function:

$$G^*(\omega) = G_s(\omega)[1 + j\eta(\omega)], \tag{1}$$

$$\eta(\omega) = \frac{G_l(\omega)}{G_s(\omega)}, \tag{2}$$

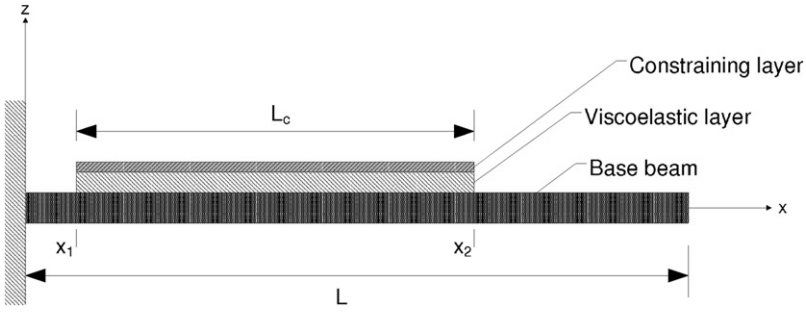


Fig. 1. Base beam with partial constrained viscoelastic layer damping.

where $G_s(\omega)$ and $G_l(\omega)$ are the storage and loss moduli, respectively, $\eta(\omega)$ is the loss factor and $\omega$ is the circular frequency. It is important to note that the moduli and loss factor are frequency dependent, as shown in Eqs. (1) and (2).

The system displacements are defined as follows:

(1) $w(x,t)$ is the transverse displacement of the system along the $z$-axis.
(2) $u_b(x,t)$ is the longitudinal displacement of the base beam along the $x$-axis.
(3) $u_c(x,t)$ is the longitudinal displacement of the constraining layer along the $x$-axis.

Here, $u_c$ and $u_b$ are independent from one another as stated by Cai et al. [7]. Fig. 2 represents a small element of the system where $\gamma_1$ is the angle of the neutral axis of the base and constraining layers with respect to the $x$-axis, and $\gamma_2$ accounts for the shear deformation of the viscoelastic layer.

Noting that for small angles, $\sin(\gamma) \approx \gamma$, and also that $\gamma_1 \simeq \partial w/\partial x$, it can be shown, using the displacements of points B and C, that

$$\gamma_2 = \frac{u_c - u_b}{h_v} + \frac{1}{h_v}\left(h_v + \frac{h_c}{2} + \frac{h_b}{2}\right)\frac{\partial w}{\partial x}. \tag{3}$$

Combining the three independent displacements $w(x,t)$, $u_b(x,t)$, $u_c(x,t)$ and Eq. (3), it is possible to define all the deformations involved in the model.

### 2.2. Energies

We will now analyze the various sources of kinetic and potential energies in the system.

*Potential energy in the viscoelastic layer*: As stated before, the central layer is made of a viscoelastic material characterized by a complex shear modulus $G^*$. It is assumed that this layer is a shear deformable body so that the potential energy involved can only arise from shear in the $xz$-plane. This deformation is noted as $\gamma_2$ and is defined by Eq. (3). The potential energy is then

$$V_v^* = \frac{1}{2}G^* h_v B \int_{x_1}^{x_2} \gamma_2^2 \, \mathrm{d}x. \tag{4}$$

*Potential energy in the elastic beams*: Both the base beam and the constraining layer are elastic beams experiencing flexural and longitudinal motions. In such beam, the potential energy due to both deformations is [23]

$$V_\alpha = \frac{E_\alpha B h_\alpha}{2}\int_{L_\alpha}\left(\frac{\partial u_\alpha}{\partial x}\right)^2 \mathrm{d}x + \frac{E_\alpha I_\alpha}{2}\int_{L_\alpha}\left(\frac{\partial^2 w}{\partial x^2}\right)^2 \mathrm{d}x, \quad \alpha \equiv b, c, \tag{5}$$

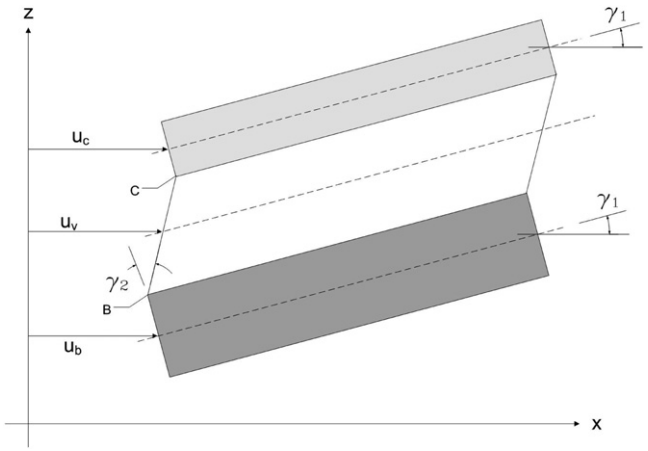


Fig. 2. Deformed element with displacements.

where $b$ and $c$ represent the base beam and the constraining layer, respectively; $E_\alpha$ is Young's modulus and $I_\alpha$ is the second moment of the section which, for a rectangular section, is $Bh_\alpha^3/12$. The integral limits $L_\alpha$ are from 0 to $L$ for the base beam and from $x_1$ to $x_2$ for the constraining layer.

The total energy of deformation is given by

$$V^* = V_v^* + V_b + V_c. \tag{6}$$

*Kinetic energy*: The kinetic energy of each layer mainly results from the transverse motion along the $z$-axis. The longitudinal and rotational kinetic energies are neglected. Also, it is assumed that all points on a cross section of the beam have the same velocity. The expression is then

$$T = T_v + T_b + T_c, \tag{7}$$

where

$$T_\beta = \frac{1}{2}\rho_\beta h_\beta B \int_{L_\beta} \left(\frac{\partial w}{\partial t}\right)^2 \mathrm{d}x, \quad \beta \equiv b, c, v.$$

The integral limits $L_\beta$ are from 0 to $L$ for the base beam, and from $x_1$ to $x_2$ for the constraining and viscoelastic layers.

### 2.3. Discretization

The assumed modes method is used to discretize the continuous system in order to go on with the derivation of the equation of motion [6,23]. This method allows us to write the three independent displacements defined earlier as functions of time and position. So, using a vector notation (where the length of the vectors is the number of modes used):

$$w(x,t) = \sum_i^{n_w} W_i(x)\psi_i(t) = \mathbf{W}^{\mathrm{T}}\boldsymbol{\psi}, \tag{8}$$

$$u_b(x,t) = \sum_j^{n_b} U_{b,j}(x)\xi_{b,j}(t) = \mathbf{U}_b^{\mathrm{T}}\boldsymbol{\xi}_b, \tag{9}$$

$$u_c(x,t) = \sum_k^{n_c} U_{c,k}(x)\xi_{c,k}(t) = \mathbf{U}_c^{\mathrm{T}}\boldsymbol{\xi}_c, \tag{10}$$

where $W_i(x)$, $U_{b,j}(x)$ and $U_{c,k}(x)$ are the admissible functions, $\psi_i(t)$, $\xi_{b,j}(t)$ and $\xi_{c,k}(t)$ are the new generalized coordinates, and $n_w$, $n_b$ and $n_c$ are the number of modes used for the transverse motion of the system ($n_w$), the longitudinal motion of the base beam ($n_b$) and the longitudinal motion of the constraining layer ($n_c$). The use of a third set of admissible functions to represent the longitudinal displacement $u_c$ was introduced by Cai et al. [7]. If $n \to \infty$ for each of the different displacements, the response is considered to be *exact*.

Admissible functions have to satisfy all geometric (or Dirichlet) boundary conditions. Even though many arbitrary functions could do so, it is convenient to use classical mode shapes. In the present model, the mode shapes of a cantilever beam are used for $w(x,t)$ and $u_b(x,t)$, and the mode shapes of a free beam are used for $u_c(x,t)$, as given in Appendix A.

Now that the three independent displacements have been discretized, it is possible to reformulate the potential and kinetic energies developed above. Inserting Eqs. (8)–(10) into Eqs. (4)–(7) leads to

$$T = \tfrac{1}{2}\dot{\boldsymbol{\psi}}^{\mathrm{T}}[\mathbf{M}_b + \mathbf{M}_v + \mathbf{M}_c]\dot{\boldsymbol{\psi}}, \tag{11}$$

$$V_\alpha = \tfrac{1}{2}\boldsymbol{\xi}_\alpha^{\mathrm{T}}\mathbf{K}_{\alpha,1}\boldsymbol{\xi}_\alpha + \tfrac{1}{2}\boldsymbol{\psi}^{\mathrm{T}}\mathbf{K}_{\alpha,2}\boldsymbol{\psi}, \tag{12}$$

$$V_v^* = \tfrac{1}{2}\boldsymbol{\xi}_c^{\mathrm{T}}\mathbf{K}_{v,1}^*\boldsymbol{\xi}_c - \boldsymbol{\xi}_c^{\mathrm{T}}\mathbf{K}_{v,2}^*\boldsymbol{\xi}_b + \tfrac{1}{2}\boldsymbol{\xi}_b^{\mathrm{T}}\mathbf{K}_{v,3}^*\boldsymbol{\xi}_b + \boldsymbol{\xi}_c^{\mathrm{T}}\mathbf{K}_{v,4}^*\boldsymbol{\psi} - \boldsymbol{\xi}_b^{\mathrm{T}}\mathbf{K}_{v,5}^*\boldsymbol{\psi} + \tfrac{1}{2}\boldsymbol{\psi}^{\mathrm{T}}\mathbf{K}_{v,6}^*\boldsymbol{\psi}, \tag{13}$$

where $\alpha$ stands again for $b$ and $c$ and submatrices are presented in Appendix B. It should be noted that the values of submatrices $\mathbf{K}^*_{v,1}$ to $\mathbf{K}^*_{v,6}$ are complex, where the imaginary part accounts for viscoelastic shear dissipation.

### 2.4. Equations of motion

The discretization process produces a $N_{\text{dof}} = n_w + n_b + n_c$ degrees of freedom system. Since the energies are now expressed in terms of finite sets of generalized coordinates (Eqs. (11)–(13)), Lagrange's equations constitute a good way to obtain the equations of motion:

$$\frac{\partial}{\partial t}\left(\frac{\partial L^*}{\partial \dot{q}_r}\right) - \frac{\partial L^*}{\partial q_r} = Q_r, \tag{14}$$

where $r = 1, 2, \ldots, N_{\text{dof}}$, $L^* = T - V^*$ is the Lagrangian and $Q_r$ represents the generalized forces. Using the vector notation introduced above, the next three sets of equations are obtained:

$$\frac{\partial}{\partial t}\left(\frac{\partial L^*}{\partial \dot{\boldsymbol{\psi}}}\right) - \frac{\partial L^*}{\partial \boldsymbol{\psi}} = \mathbf{Q}_\psi,$$

$$\frac{\partial}{\partial t}\left(\frac{\partial L^*}{\partial \dot{\boldsymbol{\xi}}_b}\right) - \frac{\partial L^*}{\partial \boldsymbol{\xi}_b} = \mathbf{Q}_{\xi_b},$$

$$\frac{\partial}{\partial t}\left(\frac{\partial L^*}{\partial \dot{\boldsymbol{\xi}}_c}\right) - \frac{\partial L^*}{\partial \boldsymbol{\xi}_c} = \mathbf{Q}_{\xi_c}. \tag{15}$$

Again, the dissipative characteristics of the system are contained in the potential energy term—and in the Lagrangian. The external force is applied locally on the base beam, along the $z$-axis. It is a function of the $x$-position and of time: $f(x,t) = \delta(x - x_f)f(t)$. The virtual work of this force is

$$\delta\mathbb{W} = \sum_i^{n_w} \delta\psi_i(t) \int_0^L f(t)\delta(x - x_f) W_i(x)\,\mathrm{d}x, \tag{16}$$

where $Q_{\psi i} = \int_0^L f(t)\delta(x - x_f)W_i(x)\,\mathrm{d}x$ is the $i$th generalized force, so that

$$\mathbf{Q}_\psi = f(t)\mathbf{W}(x = x_f). \tag{17}$$

Vectors $\mathbf{Q}_{\xi_b}$ and $\mathbf{Q}_{\xi_c}$ are both null. In their work, Cai et al. used a harmonic force to obtain the frequency response of the system [7]. This is not the case in the present work. Instead, a Dirac function $\delta(t)$ is used which leads to the impulse response. This approach is privileged because it is the basis of the solution method presented in Section 2.5.

From Eq. (15), we obtain the equations of motion of the entire system:

$$\begin{Bmatrix} \mathbf{Q}_\psi \\ \mathbf{0} \\ \mathbf{0} \end{Bmatrix} = \begin{bmatrix} \mathbf{M}_b + \mathbf{M}_c + \mathbf{M}_v & \mathbf{0} & \mathbf{0} \\ \mathbf{0} & \mathbf{0} & \mathbf{0} \\ \mathbf{0} & \mathbf{0} & \mathbf{0} \end{bmatrix} \begin{Bmatrix} \ddot{\boldsymbol{\psi}} \\ \ddot{\boldsymbol{\xi}}_b \\ \ddot{\boldsymbol{\xi}}_c \end{Bmatrix} + \begin{bmatrix} \mathbf{K}_{b,2} + \mathbf{K}_{c,2} + \mathbf{K}^*_{v,6} & -\mathbf{K}^{*\mathrm{T}}_{v,5} & \mathbf{K}^{*\mathrm{T}}_{v,4} \\ -\mathbf{K}^*_{v,5} & \mathbf{K}_{b,1} + \mathbf{K}^*_{v,3} & -\mathbf{K}^{*\mathrm{T}}_{v,2} \\ \mathbf{K}^*_{v,4} & -\mathbf{K}^*_{v,2} & \mathbf{K}_{c,1} + \mathbf{K}^*_{v,1} \end{bmatrix} \begin{Bmatrix} \boldsymbol{\psi} \\ \boldsymbol{\xi}_b \\ \boldsymbol{\xi}_c \end{Bmatrix}. \tag{18}$$

### 2.5. Solving for transient response

In order to carry out a transient analysis of the system resulting from a general impact excitation, a solution for Eq. (18) in time domain is seeked. However, as discussed previously, most stiffness terms in Eq. (13) are better represented in the frequency domain. It is therefore proposed to solve Eq. (18) in the frequency domain by means of a Fourier transform, and to convert the solution back in the time domain. To do so, the method presented by Nashif et al. [9] for a single degree of freedom system excited by a Dirac impulse is now extended and applied to the $N_{\mathrm{dof}}$ degrees of freedom system. Applying a Fourier transform to Eq. (18) leads to the well-known form

$$(\mathbf{K}^* - \omega^2\mathbf{M})\begin{Bmatrix} \overline{\boldsymbol{\psi}} \\ \overline{\boldsymbol{\xi}_b} \\ \overline{\boldsymbol{\xi}_c} \end{Bmatrix} = \begin{Bmatrix} \overline{\mathbf{Q}_\psi} \\ \mathbf{0} \\ \mathbf{0} \end{Bmatrix}, \tag{19}$$

where the overline symbol indicates a Fourier-transformed term which is a function of frequency ($\omega$). The generalized stiffness matrix $\mathbf{K}^*$ contains frequency dependent parameters representing the viscoelastic shear modulus ($G^*$) as discussed above.

Using a Dirac impulse in Eq. (17), that is $f(t) = \delta(t)$, and solving for the generalized coordinates displacements, we have

$$\begin{Bmatrix} \overline{\tilde{\boldsymbol{\psi}}} \\ \overline{\tilde{\boldsymbol{\xi}}_b} \\ \overline{\tilde{\boldsymbol{\xi}}_c} \end{Bmatrix} = (\mathbf{K}^* - \omega^2\mathbf{M})^{-1}\begin{Bmatrix} \mathbf{W}(x = x_f) \\ \mathbf{0} \\ \mathbf{0} \end{Bmatrix}, \tag{20}$$

where the under tilde notation indicates the impulse response.

It is important to note that in the frequency domain, the real part of $G^*$ (the storage modulus) is an even function while the imaginary part (the loss modulus) is an odd function [9,13]. This is a consequence of adequately representing the behavior of a viscoelastic material. That information is the key part of the method, because it turns out that each of the generalized coordinates frequency response are composed of an even real part and of an odd imaginary part. Consequently, applying an inverse Fourier transform to Eq. (20), results in a real time domain vector $[\tilde{\boldsymbol{\psi}}\ \tilde{\boldsymbol{\xi}}_b\ \tilde{\boldsymbol{\xi}}_c]^{\mathrm{T}}$.

Inserting $\boldsymbol{\psi}$ in Eq. (8) leads to the transverse impulse response[1] $w(x,t)$. The response of the system to a general transverse impact loading $h(t)$ applied at $x_f$ is then obtained using a convolution $w(x,t) = w(x,t) * h(t)$.

However, getting $w(x,t)$ is more straightforward if the convolution theorem is used. That way, the generalized coordinates displacements are given by

$$\begin{Bmatrix} \boldsymbol{\psi} \\ \boldsymbol{\xi}_b \\ \boldsymbol{\xi}_c \end{Bmatrix} = \mathscr{F}^{-1}\left(\begin{Bmatrix} \overline{\tilde{\boldsymbol{\psi}}} \\ \overline{\tilde{\boldsymbol{\xi}}_b} \\ \overline{\tilde{\boldsymbol{\xi}}_c} \end{Bmatrix} \cdot \begin{Bmatrix} \overline{\mathbf{h}} \\ 0 \\ 0 \end{Bmatrix}\right)$$

$$= \mathscr{F}^{-1}\left((\mathbf{K}^* - \omega^2\mathbf{M})^{-1}\begin{Bmatrix} \mathbf{W}(x = x_f) \\ \mathbf{0} \\ \mathbf{0} \end{Bmatrix} \cdot \begin{Bmatrix} \overline{\mathbf{h}} \\ \mathbf{0} \\ \mathbf{0} \end{Bmatrix}\right), \tag{21}$$

[1] Applying a Fourier transform to $\tilde{w}(x,t)$ leads to the complex frequency response $\overline{\tilde{w}}(x,\omega)$ of the system which can be used to get the natural frequencies.

where $\mathscr{F}^{-1}$ is the inverse Fourier transform operator and $(\cdot)$ is a point-wise multiplication. Inserting Eq. (21) in Eq. (8) leads to $w(x,t)$. Numerically, this approach is less time consuming than using a convolution.

### 2.6. Numerical computations

Based on the information given in the preceding section, it is possible to compute the transverse response $w(x,t)$ of the system submitted to a general impact. To do so, the following steps are implemented using *Matlab*:

(1) The desired time increment $\Delta t$ and the number of points of the simulation $N$ are fixed so that the total simulation time is $T_{\max} = N\Delta t$.
(2) According to the sampling theorem, the sampling frequency is given by $f_s = 1/\Delta t$ which has to be greater than twice the maximum frequency (in Hz) of the signal in order to respect the Nyquist theorem. Thus, the maximum circular frequency is $\Omega = \pi f_s$.
(3) The frequency domain $[-\Omega, \Omega]$ is discretized using $\Delta\omega = 2\pi/T_{\max}$.
(4) The forcing function $h(t)$ is sampled and transformed by using a fast Fourier transform and the result $\overline{h}$ is inserted into Eq. (21).
(5) For any given value of $\omega$ over the frequency domain, the mass and stiffness matrices are wholly determined in Eq. (21). The generalized coordinates displacement vector is found by means of linear algebra and inverse fast Fourier transform computations.
(6) Eq. (8) is applied. The result represents the transverse time response of the system to a general impulse with a time increment $\Delta t$.

### 2.7. Viscoelastic properties

To ensure an accurate representation of the core layer both in the frequency and time domains, viscoelastic properties are accounted for using Prony Series representation with $N_p$ terms. Hence, in the frequency domain

$$G^* = G_0 - G_0 \sum_{n=1}^{N_p} g_n + \sum_{n=1}^{N_p} \frac{G_0 g_n \tau_n \mathrm{j}\omega}{1 + \tau_n \mathrm{j}\omega}, \tag{22}$$

where $\tau_n$ and $g_n$ are the material specific parameters and $G_0 = G(t=0)$ is the instantaneous relaxation modulus. These parameters are obtained by using stress relaxation tests. Recalling that $G_s = \Re(G^*)$ and $G_l = \Im(G^*)$, we get the same form as expected from Eq. (1).

## 3. Model validation

In order to validate the model developed in Section 2, experiments were carried out to obtain the transient response of a beam with a wide selection of damping treatment parameters. The objective is to show the validity of the method for partial constrained viscoelastic layer damping geometry which could be used in real applications.

### 3.1. Experimental setup

Overall, 15 cantilever beams with different damping pads were tested. For each configuration, the base beam length and the damping treatment geometrical characteristics are listed in Table 1. Material properties are shown in Tables 2 and 3. All layers have a width of 25.4 mm. Both the base beam and the viscoelastic layer are 3.175 mm ($\frac{1}{8}$ in) thick while the constraining layer is 1.587 mm ($\frac{1}{16}$ in) thick. These are much thicker values than those found in the literature (see for instance Kung and Singh [4]). All three layers were bonded using a *Loctite* adhesive. The viscoelastic material was the *Urethane CPA*-850 from *Rhino Hyde Products*.

The system was submitted to a frequency sweep test. An electromagnetic exciter was used to force the harmonic transverse motion of the beam. The system response was observed using a *Bently Nevada Proximity*

Table 1
Beam specimens

| Beam | $L$ | $L_c$ | $x_1$ | $x_2$ |
|---|---|---|---|---|
| I | 508 | 375 | 15 | 390 |
| II | 511 | 375 | 68 | 443 |
| III | 510 | 250 | 78 | 328 |
| IV | 507 | 125 | 140 | 265 |
| V | 508 | 125 | 195 | 320 |
| VI | 508 | 125 | 242 | 367 |
| VII | 506 | 125 | 297 | 422 |
| VIII | 508 | 76 | 165 | 241 |
| IX | 507 | 76 | 215 | 291 |
| X | 507 | 76 | 269 | 345 |
| XI | 508 | 76 | 321 | 397 |
| XII | 509 | 26 | 191 | 217 |
| XIII | 510 | 26 | 243 | 269 |
| XIV | 510 | 26 | 297 | 323 |
| XV | 510 | 26 | 345 | 371 |

All dimensions in mm.

Table 2
Physical properties of materials

| Layer | Material | $\rho$ (kg/m$^3$) | $E$ | $G_0$ |
|---|---|---|---|---|
| Base, constraint | Aluminum 3003 | 2710 | 70 GPa | – |
| Viscoelastic | Urethane CPA-850 | 1124 | – | 14.1 MPa |

Table 3
Prony Series parameters of the viscoelastic layer

| $n$ | $g$ | $\tau$ |
|---|---|---|
| 1 | 0.2 | 0.007 |
| 2 | 0.63 | 0.07 |

*Transducer System* (3300 *XL* 8 mm). For each configuration, the first three natural frequencies were established from the locations of the peaks on the frequency response spectrum. The results are shown to be in very good agreement for all beams and modes. The greatest differences between experimental and calculated natural frequencies are 1.3 Hz on the first mode ($f_1 \approx 10$ Hz), 2.8 Hz on the second mode ($f_2 \approx 65$ Hz) and 3.7 Hz on the third mode ($f_3 \approx 175$ Hz).

### 3.2. Transient response validation

The setup was used to obtain the transient time response resulting from an impact. To do so, the system was excited using an impact hammer at a constant position $x_f = 0.04$ m and the response was recorded at different locations $x_0$. The first few milliseconds of the time responses are shown as a dashed line in Figs. 3–6. The impact force was recorded so that the real force signal could be employed in the theoretical computations. The force signals are shown in Figs. 3–6 as thick dash-dot lines. Each impact lasted for approximately 1 ms with a maximum amplitude between 7 and 9 N.

Beams III, V, VI and X were tested experimentally. They represented three different damping pad lengths (Beam III [250 mm], Beams V and VI [125 mm] and Beam X [76 mm]) and different positions (see Table 1). The number of modes used in the numerical computations were $n_w = 20$ and $n_b = n_c = 10$ . The time simulations

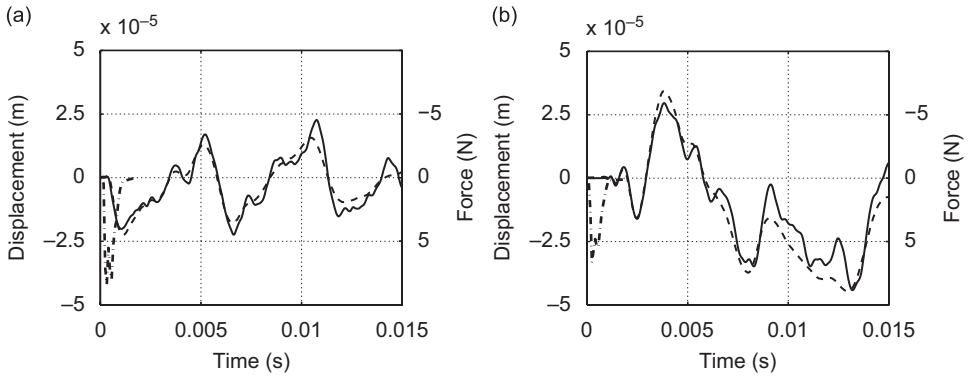


Fig. 3. Transient response of Beam III (experimental: ---, theoretical: —) and impact loading (– · –). (a) $x_0 = 0.1$, (b) $x_0 = L$.

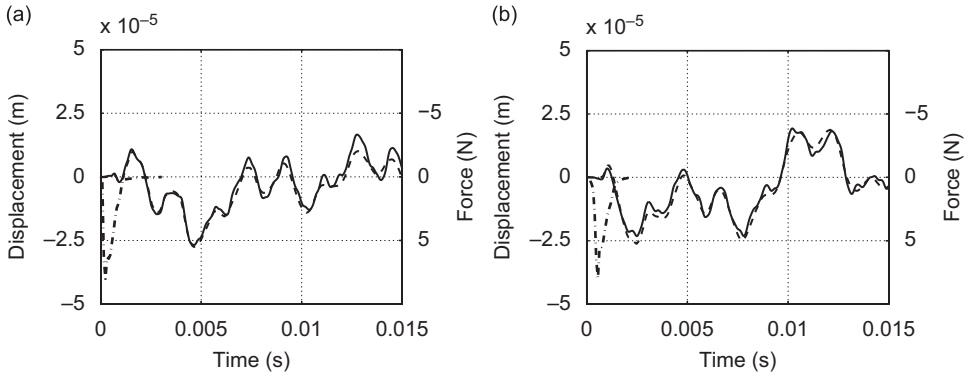


Fig. 4. Transient response of Beam V (experimental: ---, theoretical: —) and impact loading (– · –). (a) $x_0 = 0.3$, (b) $x_0 = 0.2$.

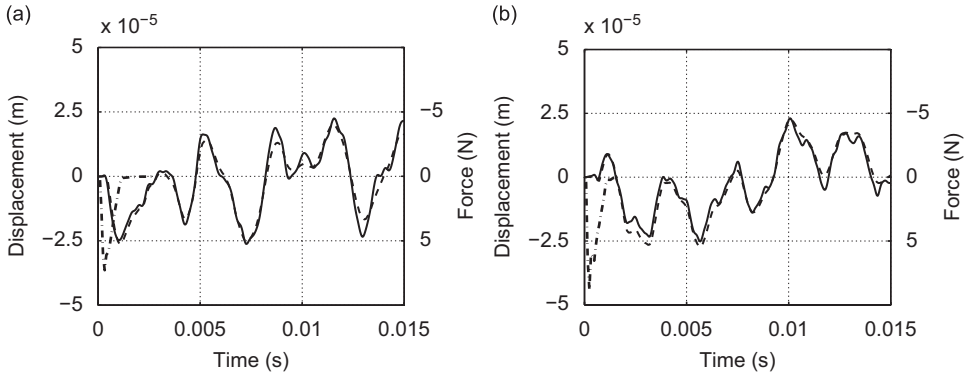


Fig. 5. Transient response of Beam VI (experimental: ---, theoretical: —) and impact loading (– · –). (a) $x_0 = 0.1$, (b) $x_0 = 0.25$.

were obtained by fixing $\Delta t = 50 \times 10^{-6}$ s and using $N = 2^{19}$ points. The numerical results are shown in Figs. 3–6 as full lines.

In Figs. 3–6, each pair of frames (a) and (b) represents the response of a single beam configuration, measured at two different locations:

(1) The transverse motions are in very good agreement with experimental data for all cases (for different observation points, patch lengths and patch positions).
(2) In Fig. 3(a), the response is measured close to the impact location and starts quickly after the beginning of the contact. On the opposite, in Fig. 3(b), the response is measured at the free end and the motion is

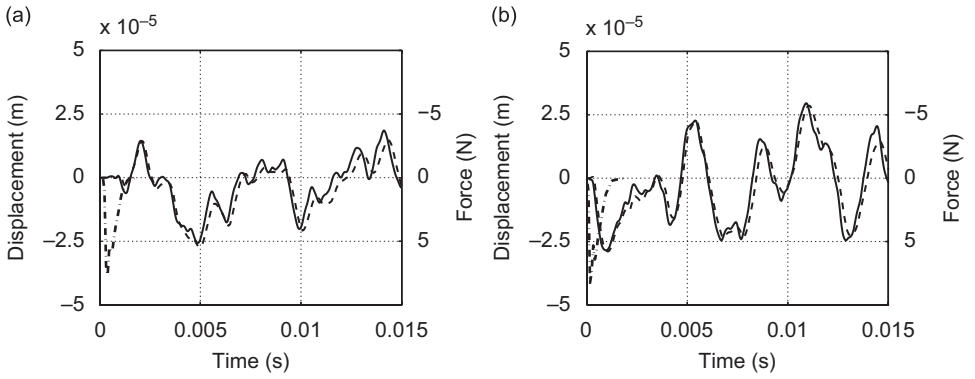


Fig. 6. Transient response of Beam X (experimental: ---, theoretical: —) and impact loading (– · –). (a) $x_0 = 0.1$, (b) $x_0 = 0.335$.

delayed with respect to the impact. Hence, wave propagation is well represented by the model since the time delay of the motion is respected between two positions.

(3) The numbers of modes used seem to depict the transverse motion quite satisfactorily.

Thus, the model is good to predict the transient transverse motion of the system for different partial constrained viscoelastic layer damping lengths and positions. Slight differences between the experimental and theoretical data may be explained by various factors. First, the impact locus in the theoretical model is a point while in the experiment, this locus is a small surface due to the impact hammer head shape. Also, the load applied in the numerical computations is perfectly perpendicular to the system. However, in the setup, it was not possible to perfectly control its direction. This may have produced oblique impacts instead of direct impacts. Besides, discrepancies may exist between the viscoelastic properties used in the analytical model and actual material values. Finally, from a design point of view, contact imperfections between layers could have occurred in the experimental setup, so that the interfaces may not have been perfectly continuous and with negligible thickness as assumed in the model.

It has been shown from experimental data that the present model and solution method are well suited to predict transient motions of beams with partial constrained viscoelastic layer damping treatments.

## 4. Numerical results

The main advantage of having an accurate and validated numerical model is that it is possible to conduct many tests without an experimental setup. System parameters can be easily modified and their effect on the general response is quickly known. In our case, each simulation took about 230 s using a 2.66 GHz dual core Intel processor and 3.25 GB of RAM. Some numerical results are now presented.

### 4.1. Geometric and physical parameters of the system

An aluminum cantilever beam ($L = 0.5$ m, $h_b = 3.175$ mm, $B = 25.4$ mm) with partial constrained viscoelastic layer damping was simulated. The system parameters were the length ($L_c$) and position ($x_1$) of the damping pad, the viscoelastic layer thickness ($h_v$) and the constraining layer thickness ($h_c$). The materials were the same as in the experimental validation (Tables 2 and 3).

### 4.2. Impact load and numerical parameters

The impacts recorded in Section 3 varied somewhat in the experiments. However, as shown in Fig. 7, if the force is normalized according to its maximum value, the different shapes are quite similar: a quick increase up to a maximum value and a slower decrease until the force disappears. According to Goldsmith, the impact force shape depends on the radius of the disturbance during the contact [26] which, in turn, depends on the

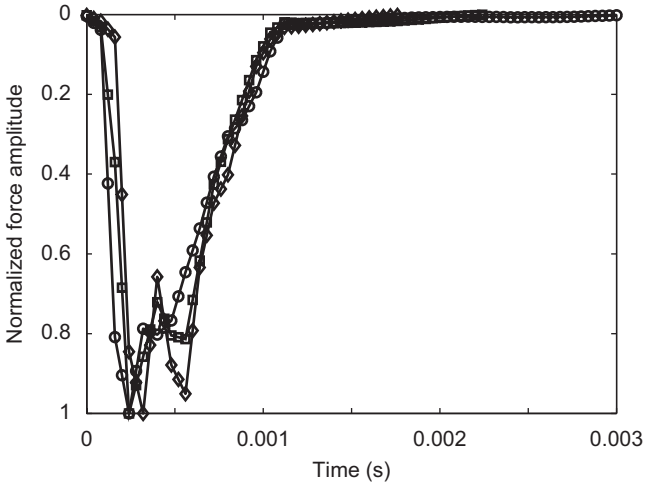


Fig. 7. Experimental impact forces. Beam III, $x_0 = L$ (-◇-). Beam III, $x_0 = 0.1$ (-▫-). Beam V, $x_0 = 0.3$ (-○-).

stiffness and mass of the impacted structure. If the damping treatment is close enough to the impact point, the added stiffness and mass could play a role in the shape of the initial deformation so that the impact force would be modified. However, since all experimental force shapes are similar, it is concluded that partial constrained viscoelastic layer damping has little influence on the shape of the force signal. In order to use the same theoretical force for all numerical examples, the impact load was defined as [24]

$$F(t) = F_0 \cdot \Re\left\{\left(\frac{1.1}{1+\Lambda+2\Lambda^2}\right)\cdot \sin[(0.97T)^{1.5}]\mathrm{e}^{(-0.4T)^4} + \left[\frac{1+2/\Lambda}{1+\Lambda}\right]\left[\frac{T}{T+\frac{1}{\Lambda}}\right]^{1.5}\mathrm{e}^{-T/\Lambda}\right\}, \tag{23}$$

where we used the parameters $F_0 = 25\,\mathrm{N}$, $\Lambda = 1$, $T = \pi t/\Gamma$ and $\Gamma = 1 \times 10^{-3}\,\mathrm{s}$. The maximum amplitude ($\approx 10\,\mathrm{N}$) is similar to those in the experiments. Also, the main part of the contact occurred before 1 ms and the signal practically died out after 2 ms. Fig. 8 presents a comparison of theoretical and experimental impact shapes. The full line represents the force given by Eq. (23). The experimental load recorded in the validation of Beam III (Section 3) and reprinted from Fig. 4(a) is shown with circle marker. The theoretical force is in fairly good agreement with the experimental force in Fig. 8.

We used the same numerical parameters as in Section 3 because it was shown that these led to good transient responses. The number of modes were set to $n_w = 20$ and $n_c = n_b = 10$. The time increment was $\Delta t = 50 \times 10^{-6}\,\mathrm{s}$ and we used $N = 2^{19}$ simulation points, for a simulation time of approximately 26 s.

### 4.3. Results and discussion

Figs. 9–12 show results for cantilever beams with different damping pad configurations. Every case treated is compared to the unpadded beam for which an analytical solution is available [25]. Each system was excited at the free end of the beam and the responses were recorded at the same location.

Transient responses are shown in Fig. 9 for systems with different damping pad lengths, in Fig. 10 for different viscoelastic layer thicknesses, in Fig. 11 for different constraining layer thicknesses, and in Fig. 12 for different damping treatment locations. In each case, it can be seen that the transient response is composed of two parts: The first part, which lasts for approximately 2 ms, is the forced response of the system during the impact; the second part is the free response of the system after the impact. In Figs. 9–12, an arrow indicates the time at the end of the contact, so that the responses shown to the left of the arrows are the forced responses. Remarkably, for a given force signal, the forced behavior is identical for all beams: the unpadded beam and all

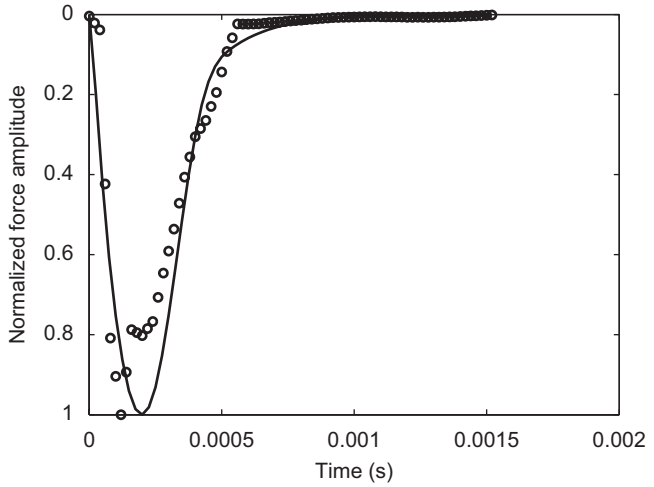


Fig. 8. Theoretical (—, Eq. (23)) and real (∘, experimental case from Fig. 4(a)) impact shapes.

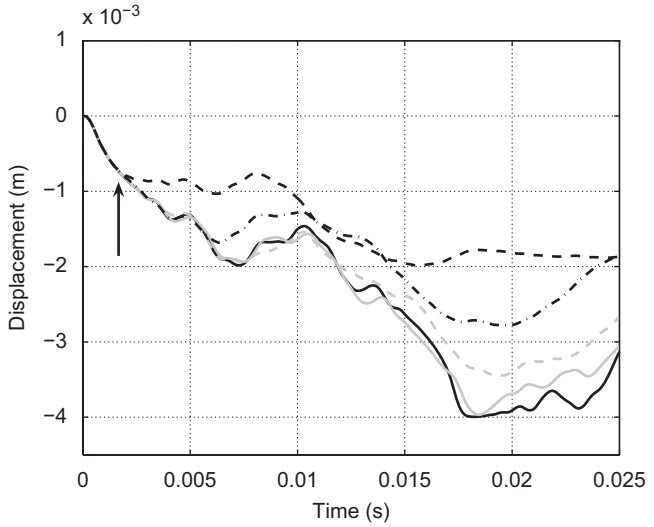


Fig. 9. Transient response for different partial constrained viscoelastic layer damping lengths. $x_f = x_0 = L$, $h_v = h_c = h_b/2$, $x_1 = 0$. $L_c = L/5$ (———), $L_c = 2L/5$ (– – –), $L_c = 3L/5$ (– · –), $L_c = 4L/5$ (- - -). Bare beam (—).

partially padded beams exhibit almost identical forced responses. It can be concluded that partial constrained viscoelastic layer damping has little effect on the forced response at the impact point of the beam.

First, the influence of the pad length is analyzed. To do so, the viscoelastic layer thickness ($h_v$), the constraining beam thickness ($h_c$) and the position ($x_1$, see Fig. 1) were fixed. The lengths used were $L_c = L/5, 2L/5, 3L/5, 4L/5$. The case where $L_c = L$ is avoided because the impact must be applied directly on the base beam and not on the damping treatment. Transient responses of the treated beams are compared to the response of the bare beam (full black line). The results are shown in Fig. 9.

We observe that beams with longer treatments have smaller amplitudes than beams with shorter treatments. For instance, the third column in Table 4 shows the relative difference on the amplitude of each padded beam with respect to the bare beam at $t = 0.02$ s. We clearly see that this difference increases with the damping pad length $L_c$. In the second column of Table 4, root mean square values over the 25 ms are shown. Again, a similar pattern is observed: overall, root mean square values are higher for shorter damping treatments.

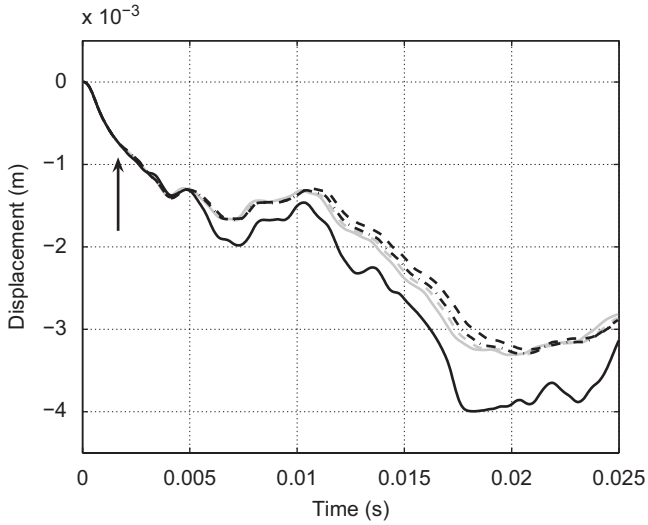


Fig. 10. Transient response for different viscoelastic thicknesses. $x_f = x_0 = L$, $h_c = h_b/2$, $x_1 = L/5$, $L_c = 2L/5$. $h_v = h_b/2$ (———), $h_v = 3h_b/4$ (– – –), $h_v = h_b$ (– · –), $h_v = 3h_b/2$ (- - -). Bare beam (—).

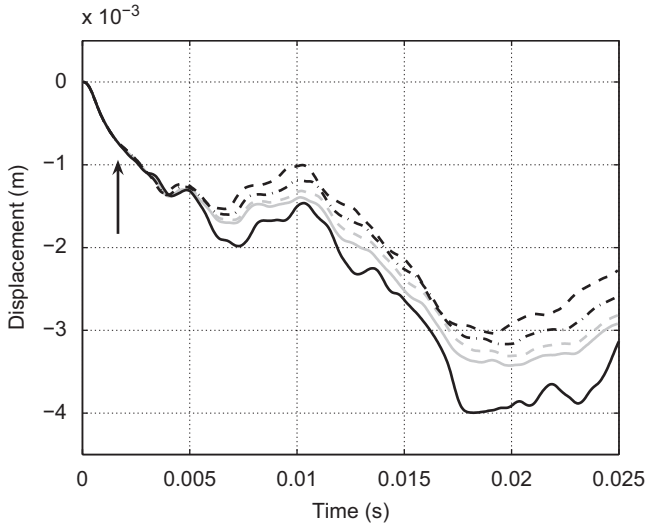


Fig. 11. Transient response for different constraining layer thicknesses. $x_f = x_0 = L$, $h_v = h_b/2$, $x_1 = L_c = 2L/5$. $h_c = h_b/4$ (———), $h_c = h_b/2$ (– – –), $h_c = 3h_b/4$ (– · –), $h_c = h_b$ (- - -). Bare beam (—).

As mentioned above, the first part of Fig. 9 is the forced response where all beams are experiencing the same displacement. After that short moment (2 ms), the different beams are free to move with different behaviors. The time of separation will be defined as the moment when the displacement of the treated beam is no longer the same as the displacement of the bare beam. A high time of separation means that the partial constrained viscoelastic layer damping is slowly effective, while a low time of separation implies a quick action. The times of separation observed in Fig. 9 are presented in Table 4. It can be seen that longer damping treatments yield lower times of separation. In particular, the times of separation for $L_c = 4L/5$ (dashed black line) corresponds approximately to the end of contact, while the times of separation for $L_c = L/5$ (full gray line) and $L_c = 2L/5$ (dashed gray line) occur much later than the end of the forced response. Based on both the time of separation and the amplitude, it is clear that for $x_1 = 0$, a short partial constrained viscoelastic layer damping treatments treatment has a relatively poor effect on the response of the beam.

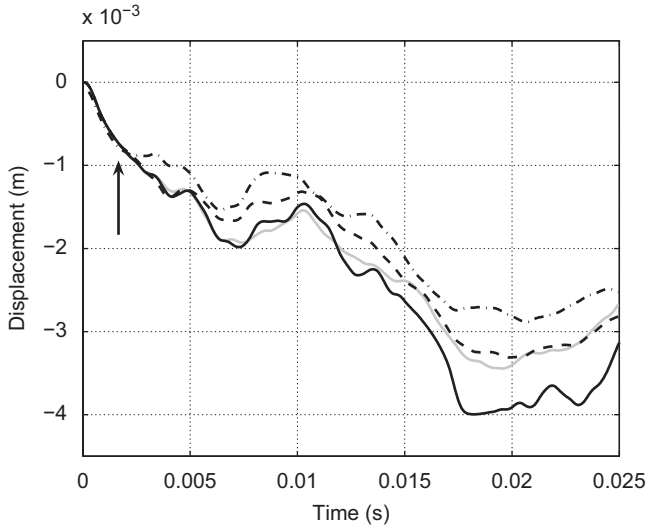


Fig. 12. Transient response for different partial constrained viscoelastic layer damping positions. $x_f = x_0 = L$, $h_v = h_c = h_b/2$, $L_c = 2L/5$. $x_1 = 0$ (———), $x_1 = L/5$ (- - -), $x_1 = 2L/5$ (– · –). Bare beam (—).

Table 4
Effect of partial constrained viscoelastic layer damping length over the amplitudes of displacement

| $L_c$ | Root mean square amplitude (m) over 25 ms | Relative difference at $t = 0.02$ s (%) | Time of separation (ms) |
|---|---|---|---|
| Bare beam | $2.6 \times 10^{-3}$ | – | – |
| $L/5$ | $2.5 \times 10^{-3}$ | 5.6 | 19 |
| $2L/5$ | $2.3 \times 10^{-3}$ | 13.0 | 12 |
| $3L/5$ | $1.9 \times 10^{-3}$ | 29.2 | 6 |
| $4L/5$ | $1.4 \times 10^{-3}$ | 46.3 | 2 |

Fig. 10 shows the effect of different viscoelastic layer thicknesses, while the other properties were fixed ($h_c = h_b/2$, $L_c = x_1 = L/5$). In these cases, the partial constrained viscoelastic layer damping treatments seem to have a rather constant effect. After the forced response, the motion of the padded beams is very similar. The root mean square amplitudes for each viscoelastic thickness are shown in Table 5. It turns out that the root mean square values for the padded beams do not vary significantly: all damping treatments have a similar effect on the beam. The times of separation for all configurations occur approximately at the same time ($t \approx 5$ ms).

For different constraining layer thicknesses (for $x_1 = L_c = 2L/5$, $h_v = h_b/2$), the results are shown in Fig. 11. Again, the time of separation is around 5 ms for all partial constrained viscoelastic layer damping treatments. However, after separation, the amplitudes of displacement are slightly reduced for thicker damping pads, as can be seen both in Fig. 11 and in the root mean square values (see Table 6).

Finally, the length of the damping treatment, the viscoelastic thickness and the constraining layer thickness were all fixed and the effect of the patch position was studied. For the case where $L_c = 2L/5$, there were three possible values for $x_1$: 0, $L/5$ and $2L/5$. Again, it was not possible to have $L_c = 3L/5$ because the impact load would have occurred on the damping treatment. The results are plotted in Fig. 12. For the three cases, the time of separation times and root mean square values are listed in Table 7. Both the amplitudes of displacement and time of separation are lower for damping pads located farther from the clamped edge. However, for positions near the free end, the energy of deformation of the base beam is very small as compared to a position near the clamp, meaning that the shear deformation in the viscoelastic ($\gamma_2$), which is responsible for the damping, should also be small. The fact that the amplitude of displacement is smaller when a damping

Table 5
Root mean square values associated with Fig. 10

| $h_v$ | Root mean square (m) |
|---|---|
| Bare beam | $2.6 \times 10^{-3}$ |
| $h_b/2$ | $2.2 \times 10^{-3}$ |
| $3h_b/4$ | $2.2 \times 10^{-3}$ |
| $h_b$ | $2.2 \times 10^{-3}$ |
| $3h_b/2$ | $2.1 \times 10^{-3}$ |

Table 6
Root mean square values associated with Fig. 11

| $h_c$ | Root mean square (m) |
|---|---|
| Bare beam | $2.6 \times 10^{-3}$ |
| $h_b/4$ | $2.3 \times 10^{-3}$ |
| $h_b/2$ | $2.2 \times 10^{-3}$ |
| $3h_b/4$ | $2.1 \times 10^{-3}$ |
| $h_b$ | $2.0 \times 10^{-3}$ |

Table 7
Root mean square values associated with Fig. 12

| $x_1$ | Root mean square (m) | Time of separation (ms) |
|---|---|---|
| Bare beam | $2.6 \times 10^{-3}$ | – |
| 0 | $2.3 \times 10^{-3}$ | 7 |
| $L/5$ | $2.2 \times 10^{-3}$ | 5 |
| $2L/5$ | $1.9 \times 10^{-3}$ | 2 |

treatment is located far from the clamped edge is more likely to be caused by an added mass effect than by damping itself.

### 4.4. Causality

Fig. 13 shows the very beginning of the transverse motions presented in Fig. 12. The initial displacement of the beam with $x_1 = L_c = 2L/5$ (–··–) is not exactly zero as it should be (and as it is for the three other cases). This is a noncausal initial displacement implying that the system is moving *before* the impact is applied. It should be noted that the amplitude of the noncausal effect is small: less than 2% of the maximum displacement. As discussed in Section 1, noncausality may occur if the viscoelastic material properties are wrongly represented; which is not the case here because viscoelastic data were found by experiments using a real material. The causality problem in Fig. 13 comes from the use of the discrete Fourier transform in the solution.

The inverse discrete Fourier transform is a periodic function of period $\tau$. Thus, the time signal will be repeated every $\tau$ seconds implying that the value of the signal at the end of the period equals the value of the signal at the beginning of the period. This is also true for $t<0$. In our case, $\tau = T_{\max} = N\Delta t$. The system is submitted to an impact at $t = 0$, so there is no displacement at this time. However, if the response has not completely died out at the end of the simulation time ($w(x, t = T_{\max}) \neq 0$), then the simulated response $w(x, t = 0)$ is not zero and causality is not respected. Fig. 14 shows two responses simulated over $T_{\max}$ seconds for the same partial constrained viscoelastic layer damping, but located at two different positions. Fig. 14(a) represents the case where $h_v = h_c = h_b/2$, $L_c = 2L/5$ and $x_1 = 0$. The amplitude of displacement completely

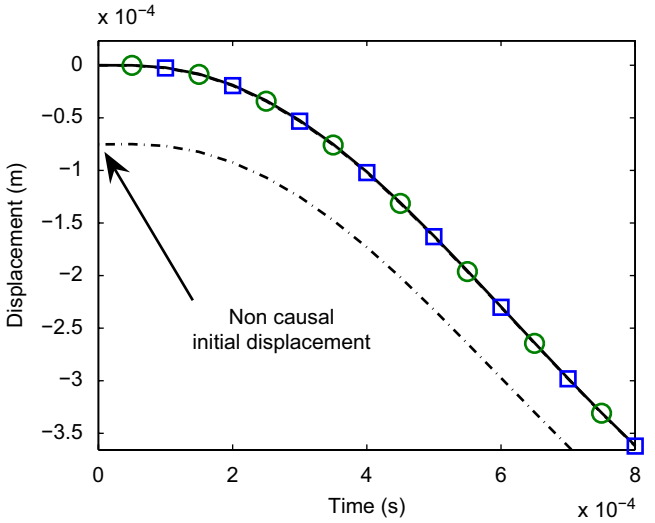


Fig. 13. Beginning of transient response for different partial constrained viscoelastic layer damping positions. $x_f = x_0 = L$, $h_v = h_c = h_b/2$, $L_c = 2L/5$. $x_1 = 0$ (-o-), $x_1 = L/5$ (-o-), $x_1 = 2L/5$ (– · –). Bare beam (—).

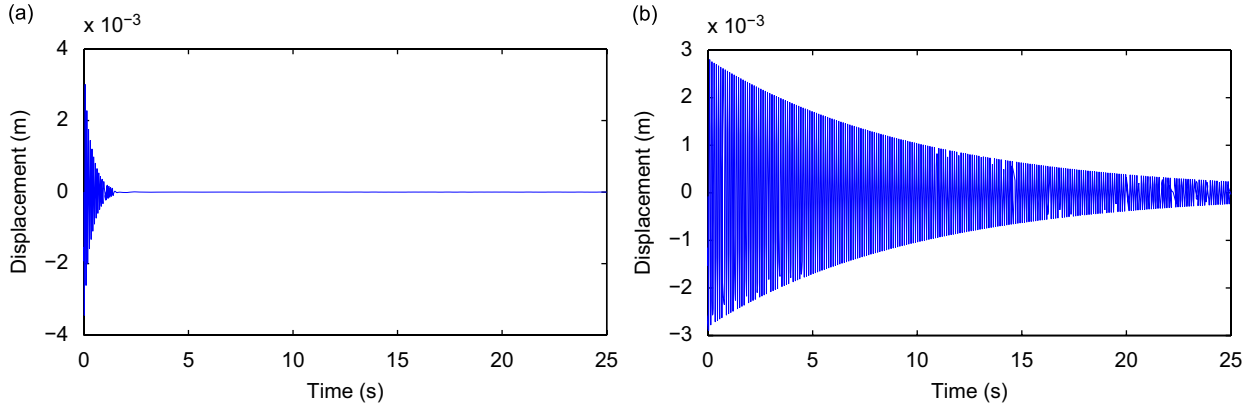


Fig. 14. Long time transient responses. $x_f = x_0 = L$, $h_v = h_c = h_b/2$, $L_c = 2L/5$. (a) $x_1 = 0$, (b) $x_1 = 2L/5$.

dies out after approximately 2 s. Consequently, this signal respects causality (see circle markers in Fig. 13). In Fig. 14(b), the damping treatment is located farther from the clamped edge, at $x_1 = 2L/5$. There are still important oscillations amplitude ($\approx 2 \times 10^{-4}$ m), even after 25 s of simulation. It is clear that this response will create a noncausal behavior as depicted in Fig. 13 (– · –).

By discrete Fourier transforming to the last 5 s of the signal presented in Fig. 14(b), we find out that the main frequency component is 9.8 Hz which corresponds to the first natural frequency of the padded beam. Therefore, in this case, the noncausality of the response is due to the fact that the partial constrained viscoelastic layer damping does not damp the first mode efficiently. In fact, the damping pad is relatively small and is located far from the clamped edge where, for the first mode shape of a cantilever beam, there is very little strain energy. As discussed earlier, this leads to a small value for the shear deformation of the viscoelastic layer. This is a problem because the viscoelastic has to experience shear deformation to dissipate energy. Without deformation, it acts more like a mass without dissipative properties. It should be pointed out that the bare beam response *is* causal although there is no damping, because displacements were obtained using a classical analytical solution instead of the Fourier transform method. The use of the Fourier transform method on the bare beam would have lead to a noncausal response for the reasons mentioned in the previous paragraph.

The perfect way to get rid of the causality problem is to increase the time of simulation to give the system all the time needed to be completely damped. However, this is time consuming and, above all, memory consuming.

## 5. Conclusion

The initial transient response of cantilever beams with partial constrained viscoelastic layer damping was studied. First, the equations of motion of the system were developed using a Lagrangian approach. The dissipative properties of the viscoelastic layer were taken into account using a Prony Series representation expressed in the frequency domain. The equations were solved in the frequency domain (leading at the same time to the natural frequencies). The responses were converted back in the time domain using inverse fast Fourier transforms, resulting in the transverse transient response of the system due to a general impact force. The transient responses were validated based on experiments. It was shown that the presented work is very well suited to represent cantilever beams with many different partial constrained viscoelastic layer damping configurations, in particular for thick viscoelastic layers.

Some numerical computations were conducted in order to observe the effects of the four geometric parameters of the damping treatment (the length, $L_c$, the position, $x_1$, the viscoelastic layer thickness, $h_v$ and the constraining layer thickness, $h_c$). Transient responses of the padded beams were compared to the response of the unpadded beam. With these few numerical examples, it seems so far that among the four parameters tested ($L_c$, $h_v$, $h_c$ and $x_1$), the patch length has the greatest influence on the initial transverse displacement of the treated beam. The patch position also has a great influence on the initial response. However, the constraining layer thickness and the viscoelastic layer thickness seem to have little influence on the initial response.

Nevertheless, a more thorough study has to be made to better understand the effects of each of these parameters. Also, from the present research, it seems that added mass has a major effect on the initial transient response (whereas damping is very important to reduce the ringing vibrations). It will be very important to understand the influence of the added mass due to partial constrained viscoelastic layer damping on the transverse displacement reduction as compared to the viscoelastic damping effect. This will be the goal of future work.

## Acknowledgments

This work was supported by Natural Sciences and Engineering Research Council of Canada (NSERC). The authors would also like to thank the reviewers for their constructive comments.

## Appendix A. Admissible functions

(i) For the transverse motion $w(x,t)$ of the cantilever system, we use

$$W_i = \cosh(\lambda_i x) - \cos(\lambda_i x) - \sigma_i[\sinh(\lambda_i x) - \sin(\lambda_i x)], \quad i = 1, \ldots, n_w, \tag{A.1}$$

where

$$\sigma_i = \frac{\sinh(\lambda_i L) - \sin(\lambda_i L)}{\cosh(\lambda_i L) + \cos(\lambda_i L)},$$

and $\lambda_1 L = 1.875$, $\lambda_2 L = 4.694$, $\lambda_i L = (i - 0.5)\pi$, $i = 3, \ldots, n_w$.

(ii) For the base beam motion along the $x$-axis, we use the longitudinal mode shapes of a cantilever beam:

$$U_{b,j} = \sin\left[\frac{(2j-1)\pi x}{2L}\right], \quad j = 1, \ldots, n_b. \tag{A.2}$$

(iii) Finally, the constraining layer is treated as a free–free beam in the longitudinal direction. So the admissible functions are given by

$$U_{c,k} = \cos\left[\frac{(k-1)\pi x}{L_c}\right], \quad k = 1, \ldots, n_c. \tag{A.3}$$

## Appendix B. Submatrices terms involved in energy expressions

$$\mathbf{M}_b = \rho_b h_b B \int_0^L \mathbf{W}^{\mathrm{T}}\mathbf{W}\,\mathrm{d}x, \tag{B.1}$$

$$\mathbf{M}_v = \rho_v h_v B \int_{x_1}^{x_2} \mathbf{W}^{\mathrm{T}}\mathbf{W}\,\mathrm{d}x, \tag{B.2}$$

$$\mathbf{M}_c = \rho_c h_c B \int_{x_1}^{x_2} \mathbf{W}^{\mathrm{T}}\mathbf{W}\,\mathrm{d}x, \tag{B.3}$$

$$\mathbf{K}_{\alpha,1} = E_\alpha B h_\alpha \int_{L_\alpha} \mathbf{U}_{\alpha,x}^{\mathrm{T}}\mathbf{U}_{\alpha,x}\,\mathrm{d}x, \tag{B.4}$$

$$\mathbf{K}_{\alpha,2} = E_\alpha I_\alpha \int_{L_\alpha} \mathbf{W}_{xx}^{\mathrm{T}}\mathbf{W}_{xx}\,\mathrm{d}x, \tag{B.5}$$

$$\mathbf{K}_{v,1}^{*} = g^{*} \int_{x_1}^{x_2} \mathbf{U}_c^{\mathrm{T}}\mathbf{U}_c\,\mathrm{d}x, \tag{B.6}$$

$$\mathbf{K}_{v,2}^{*} = g^{*} \int_{x_1}^{x_2} \mathbf{U}_c^{\mathrm{T}}\mathbf{U}_b\,\mathrm{d}x, \tag{B.7}$$

$$\mathbf{K}_{v,3}^{*} = g^{*} \int_{x_1}^{x_2} \mathbf{U}_b^{\mathrm{T}}\mathbf{U}_b\,\mathrm{d}x, \tag{B.8}$$

$$\mathbf{K}_{v,4}^{*} = \mathrm{d}g^{*} \int_{x_1}^{x_2} \mathbf{U}_c^{\mathrm{T}}\mathbf{W}_x\,\mathrm{d}x, \tag{B.9}$$

$$\mathbf{K}_{v,5}^{*} = \mathrm{d}g^{*} \int_{x_1}^{x_2} \mathbf{U}_b^{\mathrm{T}}\mathbf{W}_x\,\mathrm{d}x, \tag{B.10}$$

$$\mathbf{K}_{v,6}^{*} = \mathrm{d}^2 g^{*} \int_{x_1}^{x_2} \mathbf{W}_x^{\mathrm{T}}\mathbf{W}_x\,\mathrm{d}x, \tag{B.11}$$

$$d = \frac{2h_v + h_c + h_b}{2}, \tag{B.12}$$

$$g^{*} = \frac{G^{*}B}{h_v}. \tag{B.13}$$

## References

[1] J. Marcelin, P. Trompette, A. Smati, Optimal constrained layer damping with partial coverage, *Finite Element in Analysis and Design* 12 (1992) 273–280.
[2] D. Mead, S. Markus, The forced vibration of a three-layer damped sandwich beam with arbitrary boundary conditions, *Journal of Sound and Vibration* 10 (2) (1969) 163–175.
[3] A. Lall, N. Asnani, B. Nakra, Damping analysis of partially covered sandwich beams, *Journal of Sound and Vibration* 123 (2) (1988) 247–259.
[4] S.-W. Kung, R. Singh, Vibration analysis of beams with multiple constrained layer damping patches, *Journal of Sound and Vibration* 212 (5) (1998) 781–805.
[5] S.-W. Kung, R. Singh, Development of approximate methods for the analysis of patch damping design concepts, *Journal of Sound and Vibration* 219 (5) (1999) 785–812.

[6] S. Huang, D. Inman, E. Austin, Some design considerations for active and passive constrained layer damping treatments, *Smart Materials and Structures* 5 (1996) 301–313.
[7] C. Cai, H. Zheng, G.R. Liu, Vibration analysis of a beam with PCLD patch, *Applied Acoustics* 65 (11) (2004) 1057–1076.
[8] M. Yaman, Finite element vibration and damping analysis of a partially covered cantilever beam, *Structural Engineering and Mechanics* 19 (2) (2005) 141–151.
[9] A. Nashif, D.I.G. Jones, J. Henderson, *Vibration Damping*, Wiley, New York, 1985 (a Wiley-Interscience publication TA355 N26 1985).
[10] E. Barkanov, Transient response analysis of structures made from viscoelastic materials, *International Journal for Numerical Methods in Engineering* 44 (3) (1999) 393–403.
[11] E. Barkanov, R. Rikards, C. Holste, O. Tager, Transient response of sandwich viscoelastic beams and shells under impulse loading, *Mechanics of Composite Materials* 36 (3) (2000) 215–222.
[12] M. Slanik, J. Nemes, M. Potvin, Time domain finite element simulations of damped multilayered beams using a Prony Series representation, *Mechanics of Time-Dependent Materials* (4) (2000) 211–230.
[13] T. Pritz, Frequency dependences of complex moduli and complex Poisson's ratio of real solid materials, *Journal of Sound and Vibration* 214 (1) (1998) 83–104.
[14] R.B. Rikards, E.N. Barkanov, Determination of the dynamic characteristics of vibration-absorbing coatings by the finite-element method, *Mechanics of Composite Materials* 27 (5) (1992) 529–535.
[15] Y. Chen, Y. Xia, Z. Ren, Z. Lu, E. Wang, An optimum analysis method of sandwich structures made from elastic–viscoelastic materials, *Journal of Wuhan University of Technology—Material Science Ed* 19 (2) (2004) 76–78.
[16] G. Wang, N. Wereley, Spectral finite element analysis of sandwich beams with passive constrained layer damping, *Journal of Vibration and Acoustics* 124 (2002) 376–386.
[17] R. Moreira, J. Dias Rodrigues, Partial constrained viscoelastic damping treatment of structures: a modal strain energy approach, *International Journal of Structural Stability and Dynamics* 6 (3) (2006) 397–411.
[18] C. Vasques, B. Mace, P. Gardonio, J. Dias Rodrigues, Arbitrary active constrained layer damping treatments on beams: finite element modelling and experimental validation, *Computers and Structures* 84 (2006) 1384–1401.
[19] D. McTavish, P. Hughes, Time domain modeling of linear viscoelastic space structures, *Journal of Vibration and Acoustics* 115 (1) (1993) 103–110.
[20] M. Friswell, D. Inman, M. Lam, On the realisation of GHM models in viscoelasticity, *Journal of Intelligent Materials Systems and Structures* 18 (1997) 986–993.
[21] L. Rogers, A new algorithm for interconversion of the mechanical properties of viscoelastic materials, in: *AIAA Dynamics*, Palm Springs, USA, 1984.
[22] T. Chen, Determining a Prony Series for a viscoelastic material from time varying strain data, Technical Report (TM-2000-210123), NASA, 2000.
[23] H. Baruh, *Analytical Dynamics*, McGraw-Hill Science, Boston, 1999.
[24] W. Heitkämper, Näherungsweise Berechnung der Schallabstrahlung von storßating angeregten Platten (An approximate calculation of the acoustic radiation of impacted plates), *Acoustica* 58 (3) (1985) 141–148.
[25] B. Balachandran, E. Magrab, *Vibrations*, Thomson Brooks, Cole, Australia, Canada, 2004.
[26] W. Goldsmith, *Impact: The Theory and Physical Behavior of Colliding Solids*, E. Arnold, London, UK, 1960.